

Dalton Transactions

An international journal of inorganic chemistry

Accepted Manuscript

This article can be cited before page numbers have been issued, to do this please use: D. Vogler, N. Wolf, E. Kaifer and H. Himmel, *Dalton Trans.*, 2019, DOI: 10.1039/C9DT03151K.



This is an Accepted Manuscript, which has been through the Royal Society of Chemistry peer review process and has been accepted for publication.

Accepted Manuscripts are published online shortly after acceptance, before technical editing, formatting and proof reading. Using this free service, authors can make their results available to the community, in citable form, before we publish the edited article. We will replace this Accepted Manuscript with the edited and formatted Advance Article as soon as it is available.

You can find more information about Accepted Manuscripts in the [Information for Authors](#).

Please note that technical editing may introduce minor changes to the text and/or graphics, which may alter content. The journal's standard [Terms & Conditions](#) and the [Ethical guidelines](#) still apply. In no event shall the Royal Society of Chemistry be held responsible for any errors or omissions in this Accepted Manuscript or any consequences arising from the use of any information it contains.

Electron transfer in complexes of B^{II} cations with organic π -acceptors: A combined experimental and quantum-chemical study

View Article Online
DOI: 10.1039/C9DT03151K

Daniel Vogler, Nina Wolf, Elisabeth Kaifer, Hans-Jörg Himmel *

Abstract. Due to their combined Lewis acidity and electron-donor capability, B^{II} cations exhibit an interesting reactivity, which is almost unexplored up to date. In this work, we compare the reduction at a dicationic diborane of a series of vicinal diones with different redox potentials, namely 3,5-di-*tert*-butylbenzoquinone, 3,4,5,6-tetrachlorobenzoquinone, 1,2-naphthalene-dione, 9,10-phenanthrene-dione, 2,2'-dichlorobenzil, benzil and 1,2-acenaphthylene-dione. The experimental work is complemented by quantum-chemical calculations, illuminating the electron-transfer step in the reactions.

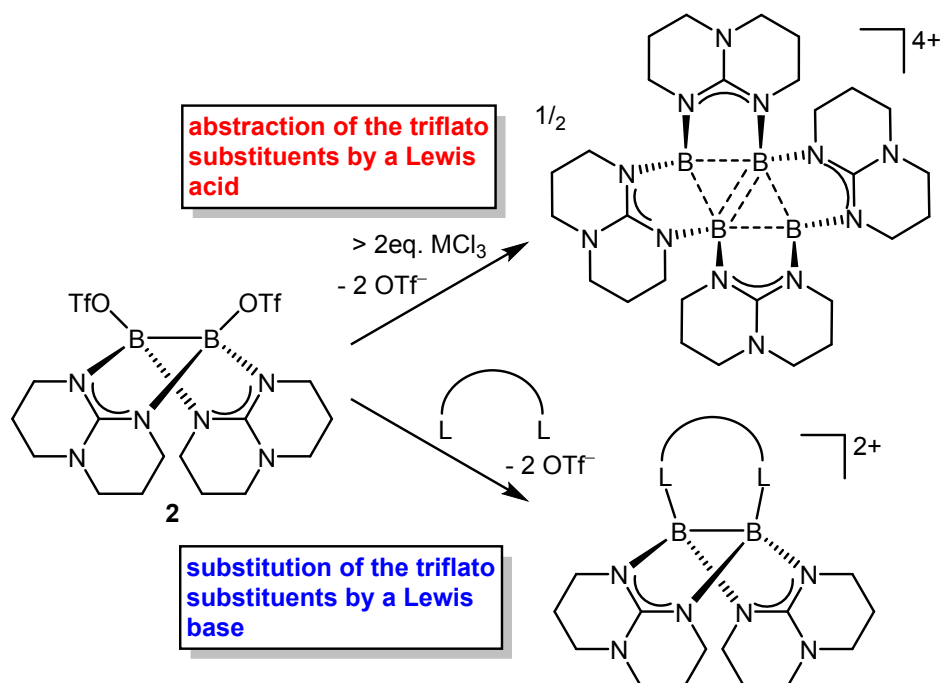
Introduction

Diborane(4) compounds are versatile reagents, that are widely applied in borylation and diboration reactions, providing convenient access to valuable intermediates in various functionalization and coupling reactions.^[1] Diborane(4) compounds with two sp²-hybridized boron atoms (sp²-sp² hybridized diboranes(4)) are generally electrophilic despite of their low boron oxidation number. In the last years several strategies were developed to modify the electrophilicity and also to turn diborane(4) compounds into nucleophiles.^[2] For example, Yamashita et al. reported the synthesis and reactivity of highly-electrophilic tetra(*o*-tolyl)diborane(4) ^[3] and the unsymmetrical diborane (4) pinB-BMes₂ (pin = pinacolato, Mes = 2,4,6-Me₃C₆H₂).^[4] Due to the high electrophilicity, tetra(*o*-tolyl)diborane(4) could even be reduced with metallic lithium or magnesium to the dianion, with double-bonded boron atoms.^[5] A few dianionic sp³-sp³-hybridized diboranes with boron-boron single bonds are also known.^[6-11] Braunschweig et al. recently reported an optimized synthetic access route to the

* D. Vogler, N. Wolf, Dr. E. Kaifer, Prof. H.-J. Himmel
Anorganisch-Chemisches Institut, Ruprecht-Karls-University of Heidelberg
Im Neuenheimer Feld 270, 69120 Heidelberg, Germany
E-mail: hans-jorg.himmel@aci.uni-heidelberg.de

tetrahalodiboranes(4) B_2X_4 ($X = \text{halogen}$) with graded electrophilicity.^[12] As to electrophilic diboranes(4), preactivated, nucleophilic neutral and anionic sp^2 - sp^3 -hybridized diboranes were obtained by addition of a carbene, an alkoxide or fluoride to a diborane(4) such as $B_2(\text{pin})_2$.^[13-15] Mahon et al. used the diboranate, resulting from reaction between a β -diketiminato magnesium *n*-butyl derivative with $B_2(\text{pin})_2$, as a source of the nucleophilic $[B(\text{pin})]^-$ in a number of reactions,^[16] including the synthesis of unsymmetrical diboranes by diborane metathesis.^[17]

Our group has synthesized an especially electron-rich neutral diborane(4) derivative $[HB(\text{hpp})]_2$ (**1**), featuring two bridging 1,3,4,6,7,8-hexahydro-2H-pyrimido[1,2-*a*]pyrimidinate (hpp) guanidinate substituents.^[18] The nucleophilicity of this compound enables catalyst-free hydroboration of CO_2 and diboration of nitriles.^[19] Moreover it allows the preparation of several unprecedented cationic oligoboranes.^[20,21] Reaction of **1** with two equivalents of methyltriflate (MeOTf) yields the diborane $[\text{TfOB}(\text{hpp})]_2$ (**2**),^[22] that was shown to be a source for $\{[B(\text{hpp})]_2\}^{2+}$ with two directly connected B^{II} cations. Double triflate abstraction from **2** with AlCl_3 or GaCl_3 gave salts of the unprecedented, fluorescent tetracation $\{[B_4(\text{hpp})_4]\}^{4+}$,^[23] exhibiting a (4c,4e) bond between the four boron atoms in the rhomboid core.



Scheme 1. Different reactions of diborane **2** with Lewis acids and Lewis bases.

Reaction of **2** with neutral σ -Lewis bases (that are π -donors or mild π -acceptors) affords a variety of dicationic diboranes and also a tetracation with two diborane units (Figure 1).^[24] In these complexes, the B-B bond length slightly decreases with increasing π -acceptor character.

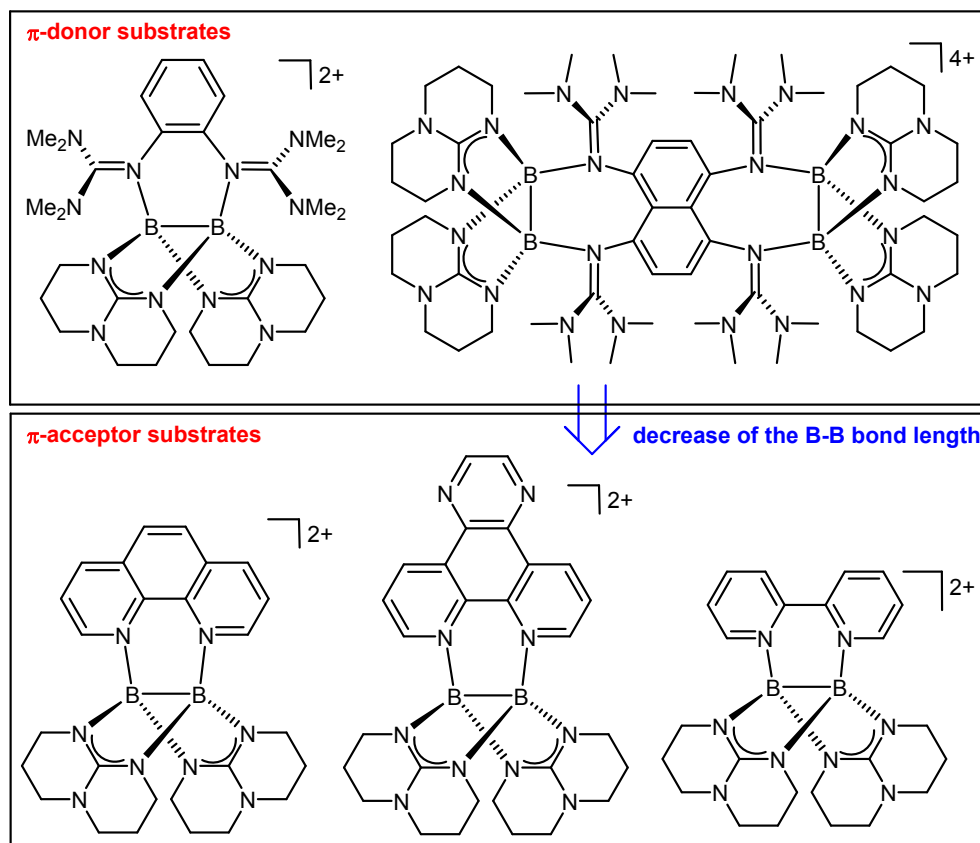
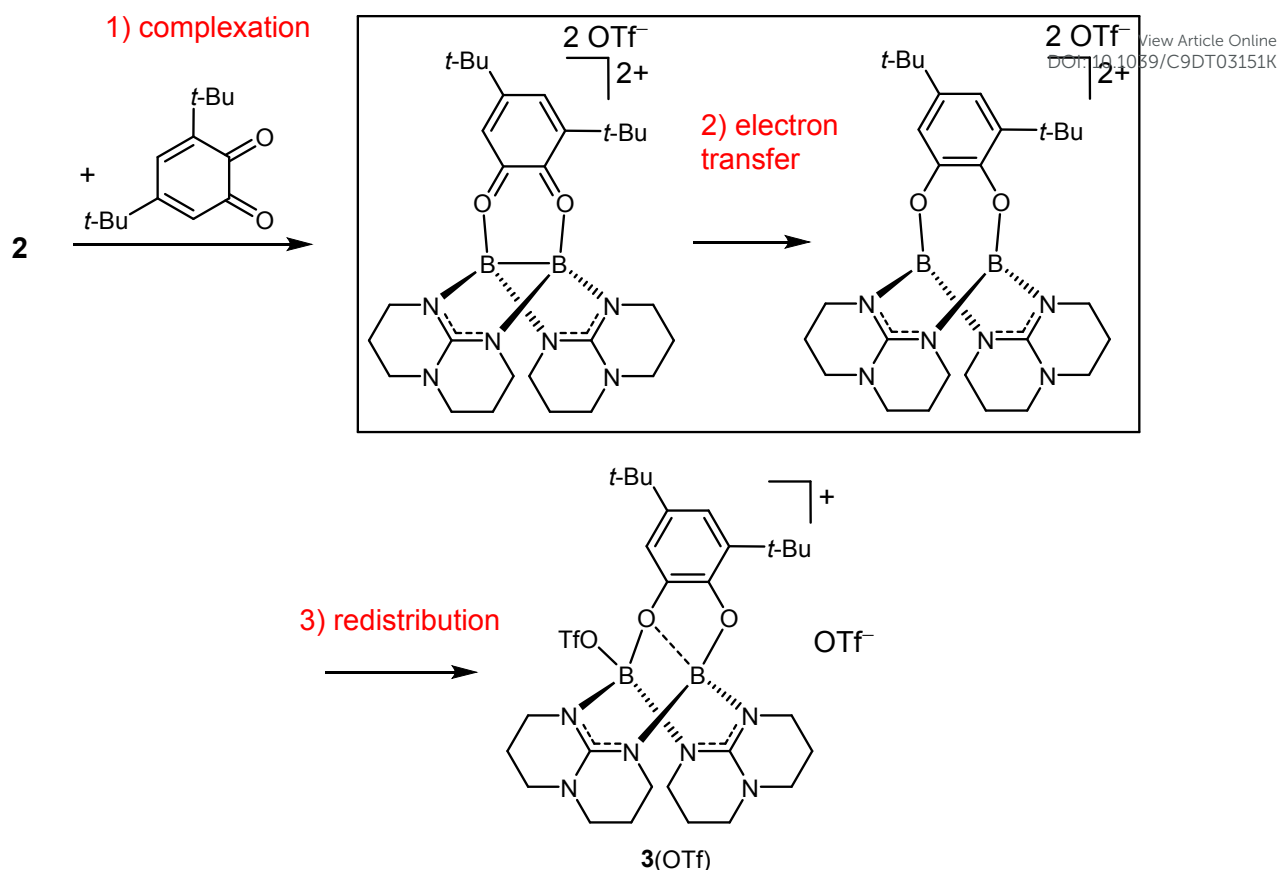


Figure 1. Fully characterized cationic boron compounds (all with triflate counterions) from previous work.

A continuative reactivity is observed if the π -acceptor character is further increased. Hence reaction of **2** with the substrate 3,5-di-*tert*-butyl-*o*-quinone (**S**₁), being a σ -Lewis base and a relatively strong π -electron acceptor, leads not only to complexation, but also to double electron-transfer from the B-B bond to **S**₁ to give the corresponding catechol complex (Scheme 2).^[24] The cleavage of the B-B bond due to B^{II} \rightarrow B^{III} oxidation initiates a redistribution process, restoring the electron octet at each boron atom to give the final product **3**(OTf) (Scheme 2).



Scheme 2. Reaction sequence leading to **3(OTf)**, comprising 1) complexation of a σ -donor/ π -acceptor, 2) electron transfer from the diborane to the π -acceptor and 3) redistribution to restore the coordination number of four at each boron atom.

Herein we systematically vary the π -acceptor strength (the redox-potential) of the dione substrate to evaluate the scope of this reactivity. The analysis of the electron-transfer step requires the application of substrates from one class of compounds, which bind in a similar way to the diboron reagent but differ in their redox-potential. To this end, the reactions of the ditriflate-diborane **2** with seven different dione substrates **S**₁ – **S**₇ (see Lewis structures in Figure 2) were compared. The redox potentials of these substrates differ considerably. Hence the $E_{1/2}$ values (vs. Fc^+/Fc) increase in the row benzil (**S**₆, -1.51 V) < 1,2-acenaphthylene-dione (**S**₇, -1.26 V) < 9,10-phenanthrene-quinone (**S**₄, -1.04 V) < 1,2-naphthalene-dione (**S**₃, -0.96) < 3,5-di-*tert*-butyl-*o*-benzoquinone (**S**₁, -0.92 V) < 3,4,5,6-tetrachloro-*o*-benzoquinone (**S**₂, -0.29 V).^[25] The experimental work is complemented by detailed quantum-chemical calculations, providing useful information about the mechanism of the electron-transfer step (concerted two-electron transfer versus two consecutive one-electron transfer steps).

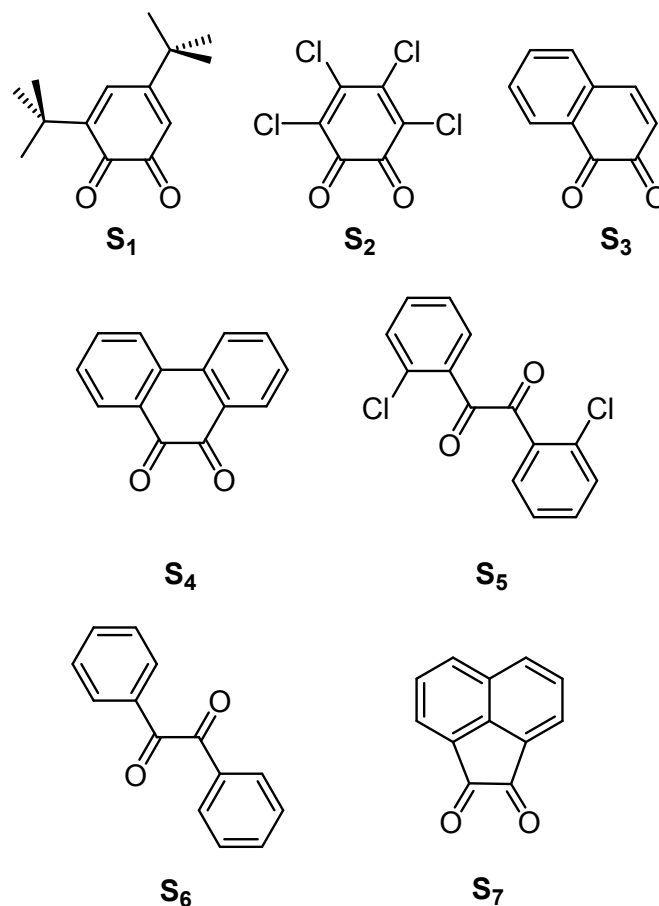
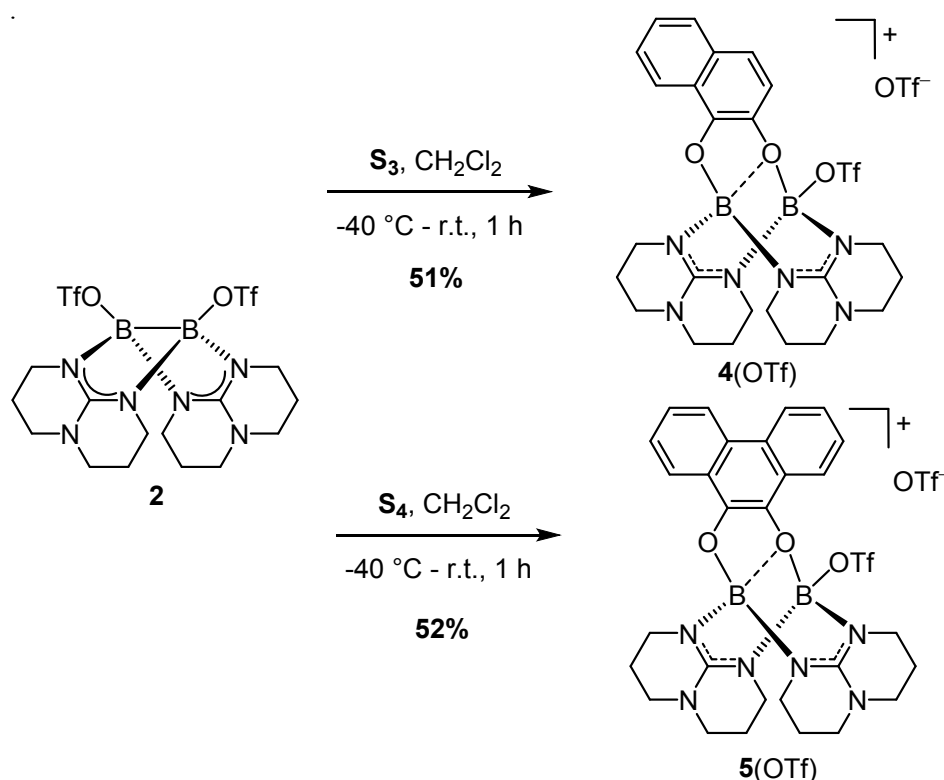


Figure 2. Lewis structures of the seven diones relevant for this study: 3,5-Ditertbutylbenzoquinone (**S**₁), 2,3,4,5-tetrachloro-benzoquinone (**S**₂), 1,2-naphthalene-dione (**S**₃), 9,10-phenanthrene-dione (**S**₄), 2,2'-dichlorobenzil (**S**₅), benzil (**S**₆) and 1,2-acenaphthylene-dione (**S**₇).

Results and Discussion

Experimental work. First we reacted diborane **2** with 1,2-naphthalene-dione (**S**₃). The two reactants were mixed at low temperature (-40 °C) in CH₂Cl₂ solution and the reaction mixture then allowed to warm up to room temperature and stirred for 1 h. The product **4**(OTf) crystallized at -20 °C in a yield of 51% after partial solvent removal (Scheme 3). The experimental solid state structure is illustrated in Figure 3a. A triflate group is bound to one of the boron atoms. Due to the bridging position of one of the oxygen atoms of reduced **S**₃, each boron atom is bound to four atoms. The boron atoms are separated by 2.443 Å, indicating that the B-B bond (c.f. 1.708(4) Å in **2** [22] and 1.772(3) Å in **1**) [26] is completely cleaved. The inset in Figure 3a highlights the large tilt of the naphthalene plane with respect to the O1-B1-O2 plane,

leading to a B1-O1-O2-C16 torsion angle of 150.26°. This conformation is presumably important to maintain a low barrier for electron transfer between the B-B bond and the organic π -system in the complex. The structure is preserved in solution. Hence the ^{11}B NMR spectrum shows two boron signals at $\delta = 6.5$ and 2.4 ppm. Using simple DFT (BP86/def2-SV(P)) calculations, the chemical shifts of the two boron atoms were calculated to be $\delta = 6.1$ (OBO) and 1.4 (OBOSO₂CF₃) ppm, in pleasing agreement with the experiment. Two signals, at $\delta = -77.0$ ppm for bound triflate and -78.94 ppm for free triflate, are also present in the ^{19}F NMR spectrum. In the UV-Vis spectra, the broad band around 400 nm due to **S**₃ disappeared and new bands in the UV region appeared. Hence the results clearly show that **S**₃ is complexed and reduced by the diborane.

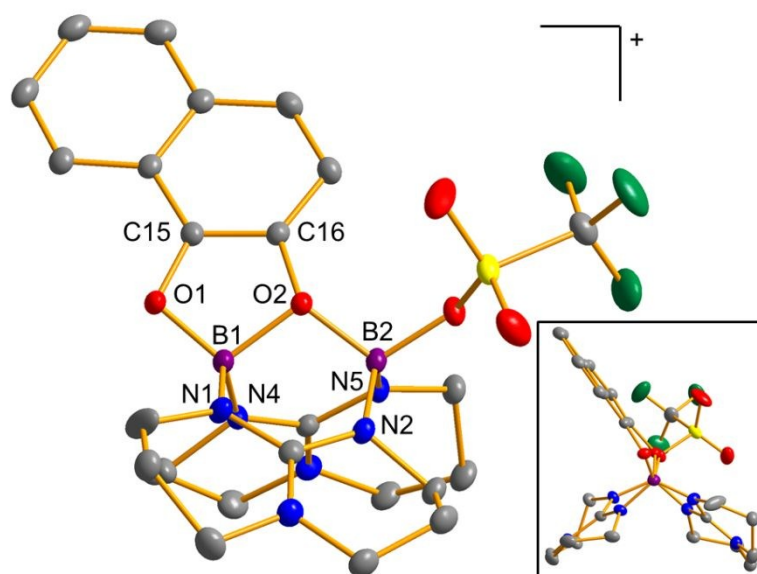


Scheme 3. Reaction of the diborane(4) [(TfO)B(hpp)]₂ (**2**) with the substrates **S**₃ and **S**₄ to give the new compounds **4**(OTf) and **5**(OTf).

Next, the reaction was repeated with 9,10-phenanthrene-quinone (**S**₄) in place for **S**₃. Reaction in CH₂Cl₂ led quantitatively to **5**(OTf) (Scheme 3), isolated by crystallization from a concentrated CH₂Cl₂ solution in a yield of 52%. The structure of **5**(OTf) is depicted in Figure 3b. The tilt of the phenanthrene plane leads to a B1-O1-O2-C16 torsion angle of 146.75°. Again, the structure is preserved in solution. Hence in the

^{11}B NMR spectrum in CD_2Cl_2 solution, two signals of equal intensity appeared at $\delta = 6.6$ and 3.1 ppm, fitting to the predicted values of $\delta = 6.5$ (OBO) and 2.3 ($\text{OBOSO}_2\text{CF}_3$) ppm from DFT (BP86/def2-SV(P)) calculations. Moreover, two signals ($\delta = -77.03$ and -79.00 ppm) show in the ^{19}F NMR spectrum in line with the structure in the solid state. Finally, the comparison between the UV-Vis spectra of **5**(OTf) and 9,10-phenanthrene-dione (**S**₄) confirms the reduction to the catechol. Hence the broad band around 350 nm in the spectrum of **S**₄ vanished and a new band at 307 nm appeared (see SI).

a)



b)

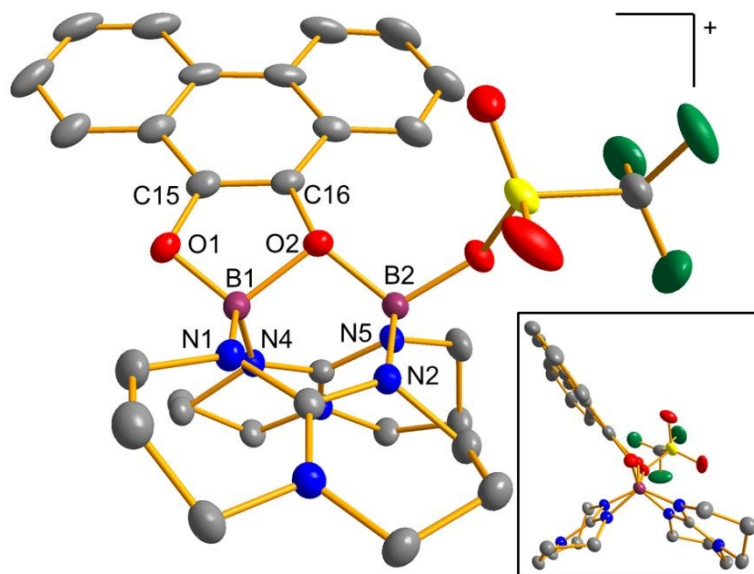
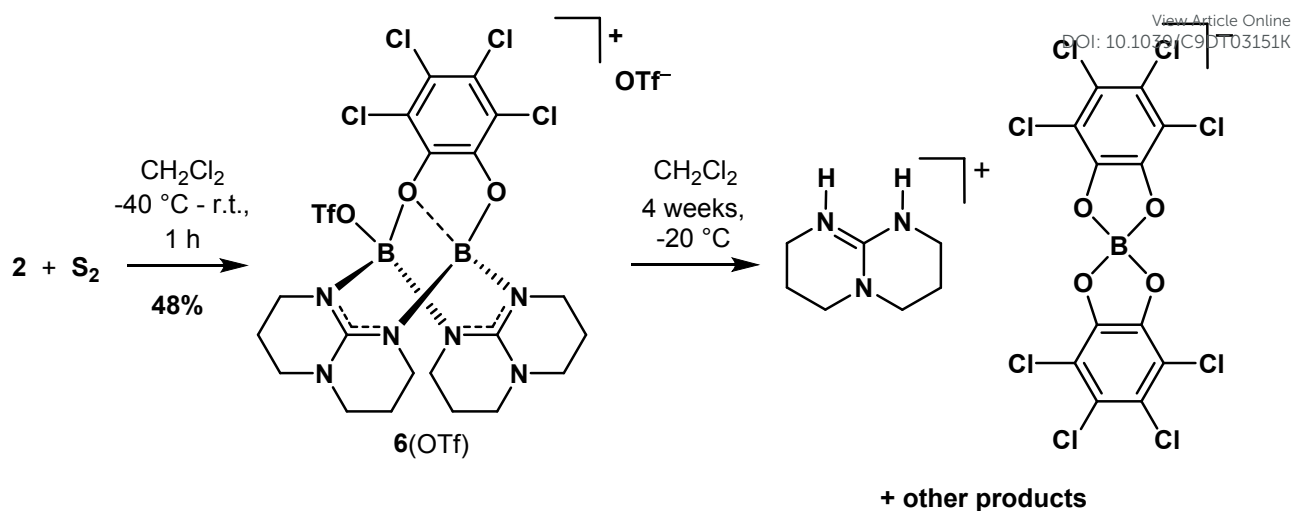


Figure 3. Illustration of the structures of the monocations **4** (a) and **5** (b) in the salts **4**(OTf)· CH_2Cl_2 and **5**(OTf)· CH_2Cl_2 . Hydrogen atoms omitted, displacement ellipsoids drawn at the 50% probability level. Selected bond distances (in Å) for **4**: B1...B2

2.443, B1-O1 1.453(1), B1-O2 1.555(2), B2-O2 1.512(2), B2-O3 1.493(2), O1-C15 1.367(2), O2-C16 1.416(2). Selected bond distances (in Å) for **5**: B1...B2 2.434, B1-O1 1.442(4), B1-O2 1.572(3), B2-O2 1.531(4), B2-O3 1.495(3), O1-C15 1.367(3), O2-C16 1.447(3). The insets show the structures along the B...B axis to highlight the tilt of the naphthalene/phenanthrene plane with respect to the O1-B1-O2 plane.

As expected from its high redox potential, reaction between **2** and 3,4,5,6-tetrachloro-*o*-benzoquinone (**S**₂) also led to substrate reduction. In the ¹¹B NMR spectrum two signals at $\delta = 7.2$ and 2.8 ppm appeared, close to the signals at $\delta = 5.6$ and 2.1 ppm reported for **3**(OTf),^[24] $\delta = 6.5$ and 2.4 ppm for **4**(OTf) and $\delta = 6.6$ and 3.1 ppm for **5**(OTf). Using DFT (BP86/def2-SV(P)) calculations, the chemical shifts of the two boron atoms were calculated to be $\delta = 6.3$ (OBO) and 1.9 (OBOSO₂CF₃) ppm. The ¹⁹F NMR spectrum showed two signals at $\delta = -77.10$ (bound triflate) and -78.97 ppm (free triflate). Moreover, the broad band at $\lambda = 456$ nm in the UV/Vis spectrum of 3,4,5,6-tetrachloro-*o*-benzoquinone was replaced by a strong absorption in the UV region at 298 nm, indicating reduction to the catechol (see SI). Hence all results confirm a reaction similar to those with **S**₁, **S**₃ and **S**₄, to give the product **6**(OTf) (Scheme 4). However, in difference to the other products, **6**(OTf) slowly decomposed in CH₂Cl₂ solutions (see SI). In an attempt to crystallize the decomposition product, the solid was washed with *n*-pentane, dissolved in CH₂Cl₂, filtrated and stored for several days at a temperature -20 °C. A few crystals precipitated in this period of time, consisting of the decomposition product (hppH₂)[B(3,4,5,6-tetrachloro-*o*-catecholato)₂] (Scheme 4, illustration of the crystal structure in the SI). The boranate ion of this salt gives rise to a sharp intense signal at $\delta = 14.1$ ppm^[27] in the ¹¹B NMR spectra of solutions of **6**(OTf) stored for 4 weeks at -20 °C, indicating its formation in larger quantities. Hence the strongly coordinating 3,4,5,6-tetrachloro-*o*-catecholato substituents replaced the hpp units, that captured two protons from the solvent or from traces of water. The presence of this decomposition product is fully consistent with oxidation of the boron atoms and reduction of the 3,4,5,6-tetrachloro-*o*-benzoquinone in the course of the reaction.



Scheme 4. Synthesis of **6(OTf)**, slowly decomposing in CH_2Cl_2 solution to give (among other unidentified products) the salt $[hppH_2][B(S_2)_2]$ with reduced substrate units.

Next we reacted compound **2** with 2,2'-dichlorobenzil (S_5) in CH_2Cl_2 solution. The ^{11}B NMR spectrum of the reaction mixture showed two signals of equal intensity at $\delta = 5.4$ and 2.2 ppm. Moreover, in the ^{19}F NMR spectrum two signals at $\delta = -76.96$ (bound triflate) and -78.97 ppm (free triflate) appeared. These results resemble those obtained for the reactions of compound **2** with S_1 - S_4 . Assuming an analogue structure for the product (denoted **7(OTf)**), the chemical shifts of the two boron atoms were calculated (BP86/def2-SV(P)) to be $\delta = 5.1$ and 0.7 ppm (see SI for more information), in good agreement with the experimental results. Hence all results indicate that **7(OTf)** exhibits a structure similar to **4(OTf)**, **5(OTf)** and **6(OTf)**. Unfortunately, it was not possible to isolate a clean reaction product. The ^{11}B NMR spectra of all products are compared in Figure 4, showing that in all cases similar products are formed.

In further experiments, we tested the possibility of eliminating the diborane unit from the reduced substrate. The three isolated products **3(OTf)**, **4(OTf)** and **5(OTf)** were dissolved in methanol and stirred for three days at $50\text{ }^\circ\text{C}$. Both NMR (see SI) and mass spectrometric data indicate for each reaction the formation of the free catechol (S_1+2H , S_3+2H and S_4+2H). However, the NMR spectra also indicate that elimination of the diborane unit is accompanied by its decomposition.

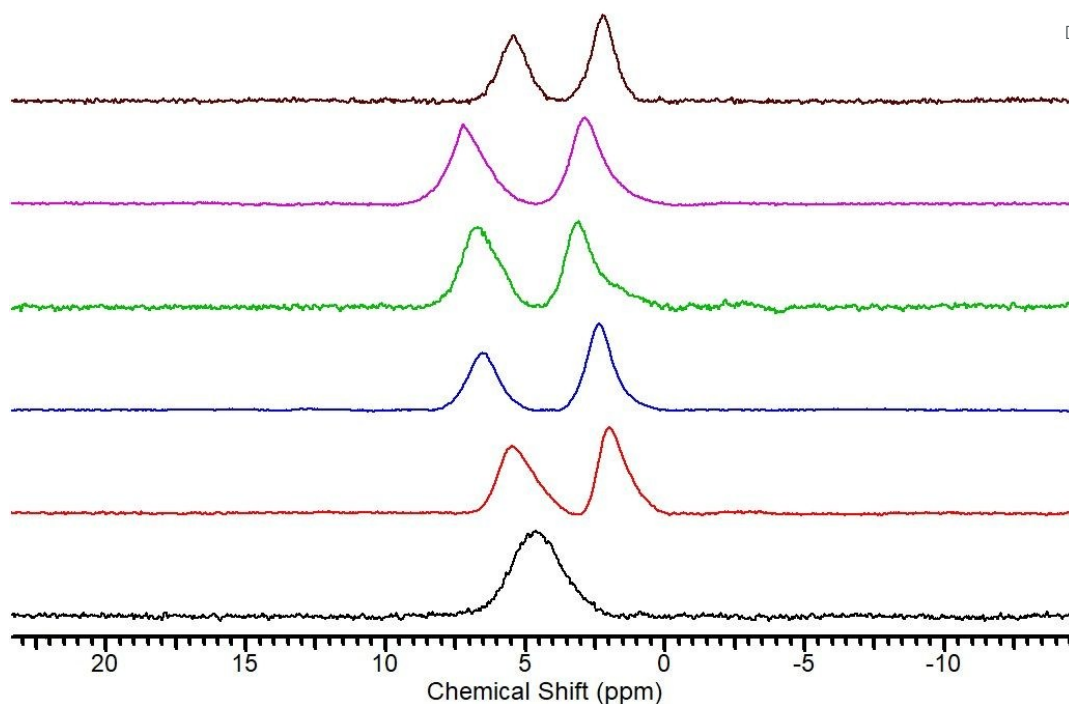
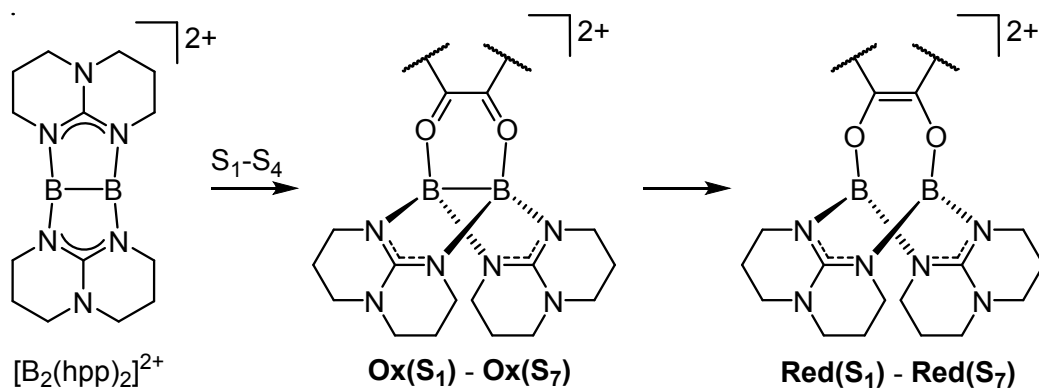


Figure 4. ^{11}B NMR spectra (128 MHz, CD_2Cl_2) for the diborane reactant **2** (black) and the products **3**(OTf) (red), **4**(OTf) (blue), **5**(OTf) (green), **6**(OTf) (magenta) and the product of the reaction of **2** with **S**₅ (brown), **7**(OTf).

Reaction of **2** with **S**₆ gave no clear results. Although the ^{11}B NMR spectrum in CD_2Cl_2 solution displayed a new signal at $\delta = 2.2$ ppm, the signal of **2** in the ^{19}F NMR spectrum remained unchanged. Unfortunately it was not possible to identify the boron species responsible for the new signal in the ^{11}B NMR spectrum. After a few days a small amount of crystals were isolated from the reaction mixture, that turned out to be the condensation product of 1,2-diphenyl-1,2-ethenediol with hppH_2^+ , crystallizing together with triflate as counter-ion (see SI for a structural characterization). Although the isolated crystals do not contain the direct product of addition of compound **2** to **S**₆, the structure of the crystallized salt still indicates reduction of the benzil during the reaction. Finally, reaction of **2** with **S**₇ also led to no clear results. Although the change of the color of the solution from orange to red indicates a reaction, the ^{11}B NMR spectrum shows no specific signals. On the other hand, several signals appeared in the ^{19}F NMR spectrum, indicating degradation of the triflate anions (see SI). This result points to the formation of reactive radical intermediates (see discussion under consideration of the theoretical results below). Unfortunately an identification of the products was not possible.

Quantum-chemical calculations. The experiments indicate that electron-transfer takes place for a variety of vicinal dione substrates with different redox-potentials, demonstrating the wide scope of this reactivity. Quantum-chemical calculations were carried out to gain further information on the electron-transfer step. In these calculations we concentrated on the reaction sequence depicted in Scheme 5. The B3LYP functional in combination with the def2-TZVP basis set was chosen for these calculations, since this method has shown previously to provide reliable results for guanidinate-bridged diborane molecules.^[18c] First the structures of the products of complexation and reduction of the substrates **S**₁-**S**₇ by the dication [B₂(hpp)₂]²⁺ (denoted **Red(S**₁)-**Red(S**₇) in the following) were calculated. Illustrations of the structures of **Red(S**₁)-**Red(S**₄) can be found in the SI, and pictures of the structures of **Red(S**₅)-**Red(S**₇) are included in Figures 5-7 (vide infra). Selected structural parameters for all products are compiled in a Table in the SI. The large separations of the two boron atoms (2.357 – 2.417 Å) indicate in all cases cleavage of the B-B bond. Moreover, the other parameters signal reduction of the vicinal diones to the corresponding catecholato forms.



Scheme 5. Reaction sequence analysed in the quantum-chemical calculations.

In Table 1, the ΔE , ΔH (0 K) and ΔG (298 K) values calculated for the reactions between [B₂(hpp)₂]²⁺ and **S**_{*n*} (*n* = 1 - 7) to give the products **Red(S**_{*n*}) are compared. All reactions are exothermic and exergonic. Interestingly, the reaction with **S**₁ ($\Delta G = -258$ kJ mol⁻¹) is more exergonic than that with **S**₂ ($\Delta G = -230$ kJ mol⁻¹), although **S**₂ clearly exhibits the higher redox potential ($E_{1/2} = -0.29$ V vs. Fc⁺/Fc for **S**₂ and -0.92 V for **S**₁). Furthermore, similar ΔG values were calculated for the reactions with **S**₆ (-132 kJ mol⁻¹) and **S**₇ (-138 kJ mol⁻¹), although **S**₆ exhibits a significantly lower redox-

potential ($E_{1/2} = -1.51$ V vs. Fc^+/Fc for \mathbf{S}_6 and -1.26 V for \mathbf{S}_7). Obviously, the lower Lewis basicity of the reduced catecholates diminishes the energy of complexation to the boron atoms, leading in the sum to a less exergonic reaction. Formation of **Red(\mathbf{S}_6)** is associated with the smallest, but still considerable negative Gibbs free energy change ($\Delta G = -132$ kJ mol⁻¹).

Table 1. Reaction energies ΔE , enthalpies ΔH at 0 K and Gibbs free energies ΔG at 298 K (all in kJ mol⁻¹) calculated with B3LYP/def2-TZVP for the reactions between $[\text{B}_2(\text{hpp})_2]^{2+}$ and the seven dione substrates \mathbf{S}_1 - \mathbf{S}_7 to give the complexed and reduced compounds **Red(\mathbf{S}_1)** - **Red(\mathbf{S}_7)**.

Reaction	ΔE	ΔH (0 K)	ΔG (298 K)
$[\text{B}_2(\text{hpp})_2]^{2+} + \mathbf{S}_1 \rightarrow \mathbf{Red}(\mathbf{S}_1)$	-331	-322	-258
$[\text{B}_2(\text{hpp})_2]^{2+} + \mathbf{S}_2 \rightarrow \mathbf{Red}(\mathbf{S}_2)$	-303	-295	-230
$[\text{B}_2(\text{hpp})_2]^{2+} + \mathbf{S}_3 \rightarrow \mathbf{Red}(\mathbf{S}_3)$	-296	-288	-224
$[\text{B}_2(\text{hpp})_2]^{2+} + \mathbf{S}_4 \rightarrow \mathbf{Red}(\mathbf{S}_4)$	-274	-267	-201
$[\text{B}_2(\text{hpp})_2]^{2+} + \mathbf{S}_5 \rightarrow \mathbf{Red}(\mathbf{S}_5)$	-245	-235	-178
$[\text{B}_2(\text{hpp})_2]^{2+} + \mathbf{S}_6 \rightarrow \mathbf{Red}(\mathbf{S}_6)$	-203	-196	-132
$[\text{B}_2(\text{hpp})_2]^{2+} + \mathbf{S}_7 \rightarrow \mathbf{Red}(\mathbf{S}_7)$	-208	-200	-138

In the case of the three substrates $\mathbf{S}_5 - \mathbf{S}_7$ (but not for $\mathbf{S}_1 - \mathbf{S}_4$), the calculations found a second minimum on the potential energy hypersurface, corresponding to the intermediates **Ox(\mathbf{S}_5)** - **Ox(\mathbf{S}_7)** prior to electron transfer. These intermediates exhibit a higher energy than the products of two-electron transfer **Red(\mathbf{S}_5)** - **Red(\mathbf{S}_7)**. The energy difference decreases in the order $\Delta E = 108$ kJ mol⁻¹ for \mathbf{S}_5 , 67 kJ mol⁻¹ for \mathbf{S}_6 and only 42 kJ mol⁻¹ for \mathbf{S}_7 . For these three substrates, we also tried to calculate the products of one-electron transfer, being biradicals with open-shell singlet or triplet states. Broken-symmetry calculations were not successful, as they converged to the structures **Red(\mathbf{S}_5)** - **Red(\mathbf{S}_7)**. On the other hand, the lowest energy triplet states, denoted **T(\mathbf{S}_5)** - **T(\mathbf{S}_7)** in the following, were successfully calculated. The calculated structures are illustrated in Figures 5 - 7. The trends in the calculated bond distances (see the numbers in the Tables integrated in Figures 5 - 7) are fully consistent with the interpretation of the triplet structures as being the products of one-electron transfer, with one unpaired electron in the B-B bond orbital ($1e2c$ bond) and another unpaired electron on the vicinal dione unit. For example, the distance between the

two boron atoms increases from 1.656 Å in **Ox(S₅)** to 1.865 Å in **T(S₅)** and finally to 2.360 Å in **Red(S₅)**. For comparison, Wagner et al. reported an increase of the B-B distance from the dianion of bis(9-borafluorenyl)methane (1.906(3) Å for a 2e2c bond) to the monoanion (2.166(4) Å for a 1e2c bond) and finally to the neutral compound (2.534(2) Å, no direct bond).^[7] Interestingly, the energies of the triplet states **T(S_n)** are for all three substrates close to those of the **Ox(S_n)** states.

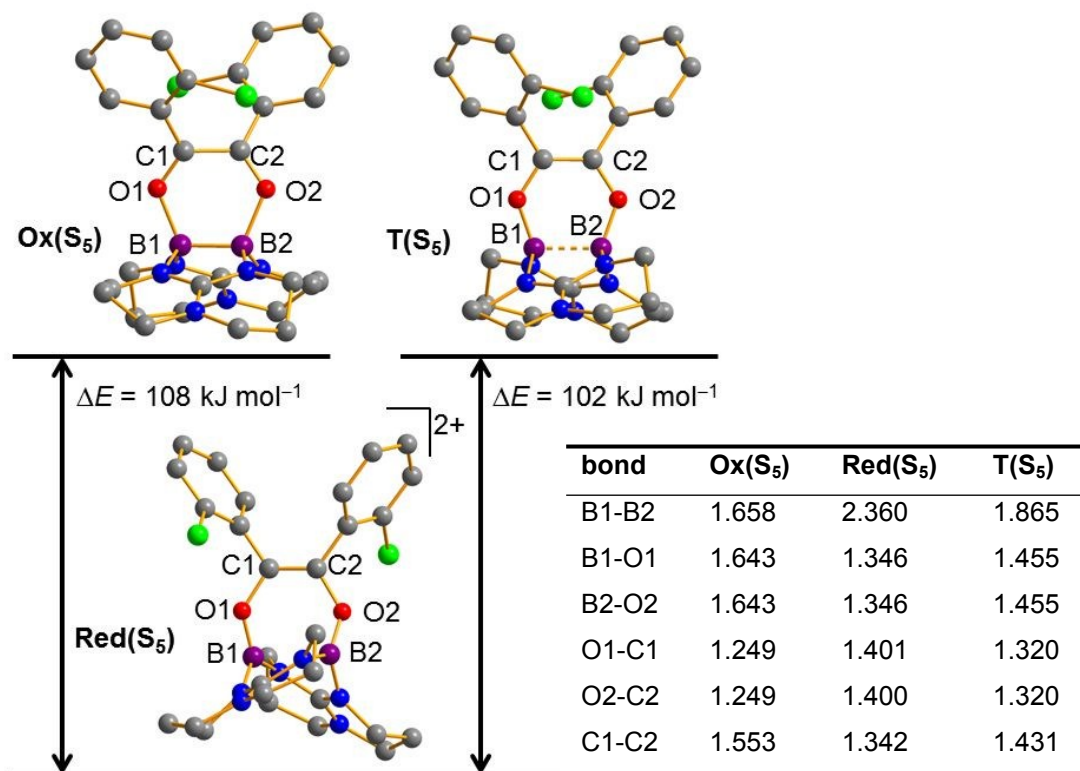


Figure 5. Structures and relative energies of the three minima **Red(S₅)**, **Ox(S₅)** and **T(S₅)**. Selected structural parameters (in Å) for the minima on the closed-shell singlet and triplet potential energy hypersurfaces are compiled in the inserted table.

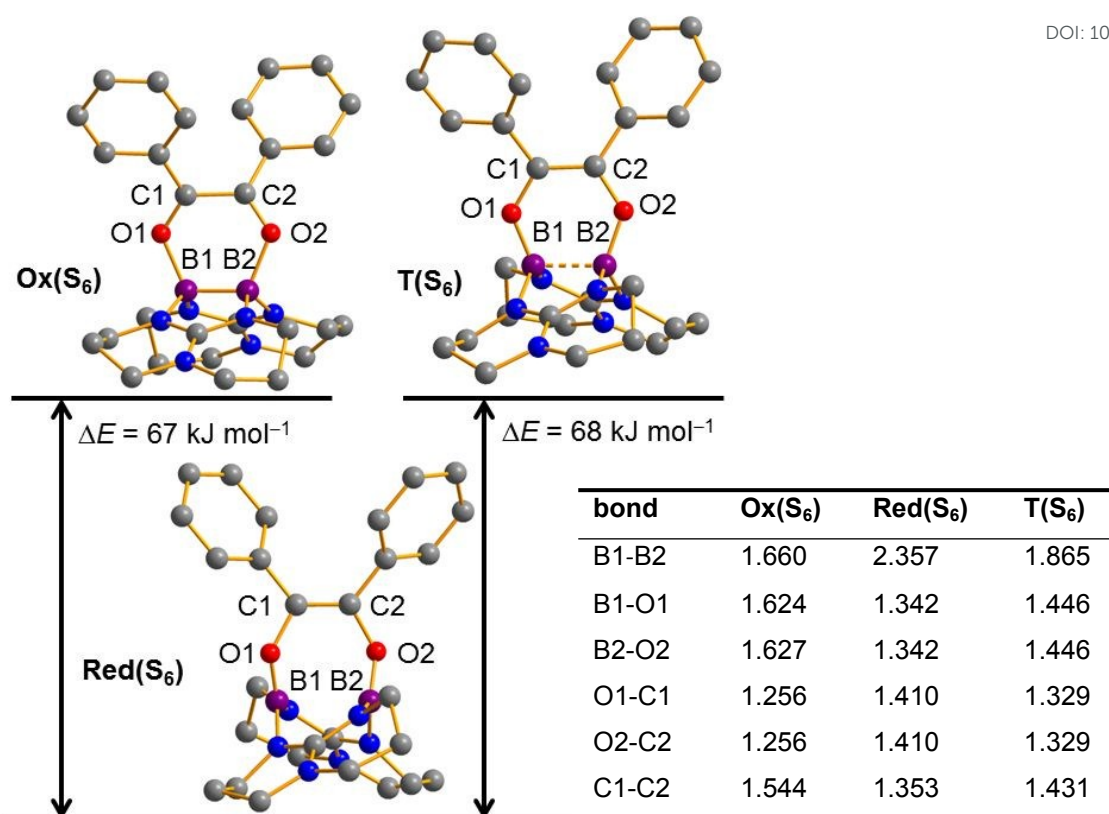


Figure 6. Structures and relative energies of the three minima **Red(S₆)**, **Ox(S₆)** and **T(S₆)**. Selected structural parameters (in Å) for the minima on the closed-shell singlet and triplet potential energy hypersurfaces are compiled in the inserted table.

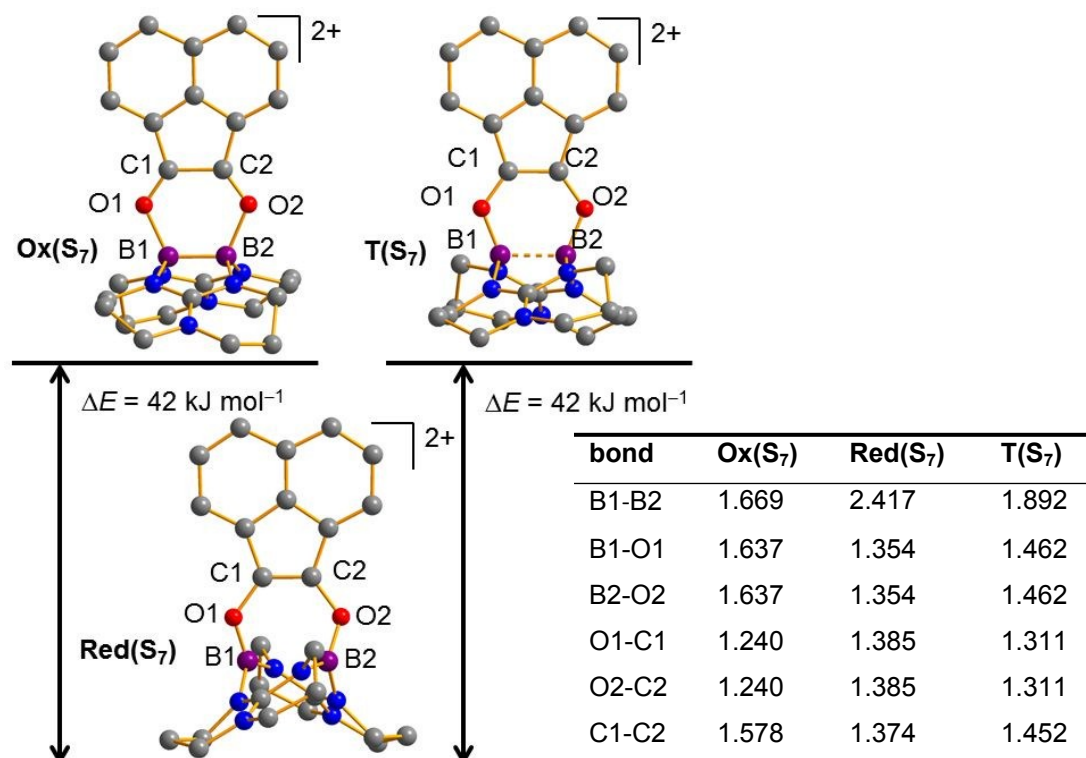


Figure 7. Structures and relative energies of the three minima **Red(S₇)**, **Ox(S₇)** and **T(S₇)**. Selected structural parameters (in Å) for the minima on the closed-shell singlet and triplet potential energy hypersurfaces are compiled in the inserted table.

The results indicate that the B-B distance could serve as adequate reaction coordinate for a further evaluation of the electron-transfer step. We therefore optimized the energies of the compounds with fixed B-B distances for several B-B distances in the range 1.5 – 2.6 Å. In the calculations carried out for **S₄** (see SI), the energy decreased until it reached a single minimum at a distance of 2.340 Å. The calculated structure at the minimum complies with the fully-optimized structure **Red(S₄)**, proving complete barrier-less two-electron transfer. There existed no further local energy minimum corresponding to the intermediate **Ox(S₄)**, but the calculations found a shallow potential energy curve in the area around a B-B distance of 1.7 Å (see SI). In the case of the three substrates **S₅** – **S₇**, the potential energy scan found the two minima that correspond to **Red(S_n)** and **Ox(S_n)**, and also provided estimates for the barriers for two-electron transfer along the singlet potential energy curves. As example, the energy relative to the **Red(S₇)** global-energy minimum is plotted in Figure 8a as a function of the B-B distance for the complex with **S₇**. One can see that a barrier of ca. 29 kJ mol⁻¹ separates the two minima **Ox(S₇)** and **Red(S₇)** on the singlet potential-energy curve. At the barrier, the B-B bond is ca. 1.95 Å long, being close to the equilibrium distance of 1.892 Å calculated for the triplet state, **T(S₇)**. Similar calculations for the substrates **S₅** and **S₆** lead to lower barriers of ca. 22 kJ mol⁻¹ for **Ox(S₆)** → **Red(S₆)** and ca. 9 kJ mol⁻¹ for **Ox(S₅)** → **Red(S₅)**. Hence the barrier height decreases with increasing absolute energy difference between the isomers with oxidized (**Ox(S_n)**) and reduced (**Red(S_n)**) substrate, and also with increasing ΔG values for the electron transfer step. Such a relationship is expected from the Marcus theory, although this theory is based on the assumption of an outer-sphere mechanism, that clearly is not fulfilled here. To further elaborate on this point, we plotted the square-root of the activation energy ΔE_a as a function of the reaction energy. Although the significance of such a plot is reduced due to the small number of data points, the almost perfect linear fit (see Figure 8b) indicates that the two-electron transfer step in these compounds complies with the behavior expected from Marcus theory. Obviously, it is not meaningful to derive a parameter λ from this plot. For the substrates **S₆** and **S₇**, the barrier for simultaneous two-electron transfer along the singlet potential energy curve is already quite high. In such cases a stepwise one-electron transfer process should be preferred, since the triplet state is significantly lower in energy in the region of this barrier. Presumably, an open-shell singlet state

lies close to this triplet state and allows the transfer of an electron without change of spin multiplicity. This process produces radical intermediates, provoking side reactions. This might explain the different results of the experiments in which S_6 and S_7 were applied. Especially the degradation of the triflate counterions in the reaction with S_7 indicates the formation of reactive radical intermediates in solution.

View Article Online
DOI: 10.1039/C9DT03151K

Conclusions

In this work, the ditriflate-substituted diborane $[TfOB(hpp)]_2$ with bridging guanidinate (hpp) substituents (compound **2**) was applied as a source for the dicationic diborane $[B_2(hpp)_2]^{2+}$, being both a Lewis acid and an electron donor. The reactions with a series of vicinal diones with different redox potentials demonstrate the ability of this dicationic diborane to complex organic substrates in the first step and reduce them in a second electron-transfer step. The two-electron reduction of the organic substrate is accompanied by loss of the boron-boron bond ($B^{II} \rightarrow B^{III}$). Quantum-chemical calculations were then applied to gain more insight into the electron-transfer step. For three substrates it was possible to locate two minima on the singlet potential-energy hypersurface corresponding to the complexed substrate before and after two-electron transfer. Moreover, the calculations show that the decrease of the energy difference between these two minima leads to an increase of the activation barrier for simultaneous two-electron transfer. The relationship between thermodynamics and kinetics of this simultaneous two-electron transfer complies with the expectations from Marcus theory (although not obeying an outer-sphere mechanism). Additional calculations show that the lowest-energy triplet state, corresponding to the product of one-electron transfer, exhibits an energy similar to that of the diborane-substrate complex before electron-transfer. This indicates that the presence of a significant barrier for the simultaneous two-electron transfer along the singlet potential energy curve leads to a change of the electron-transfer process to a pathway with stepwise transfer of the two electrons, explaining the experimental findings. Ongoing work in our laboratory aims at the isolation of redox-isomers and the synthesis of open-shell biradicals in which one unpaired electron is in the π -system of the organic substrate and the other in the B-B bond orbital. The results of this work build a solid fundament for research in these directions.

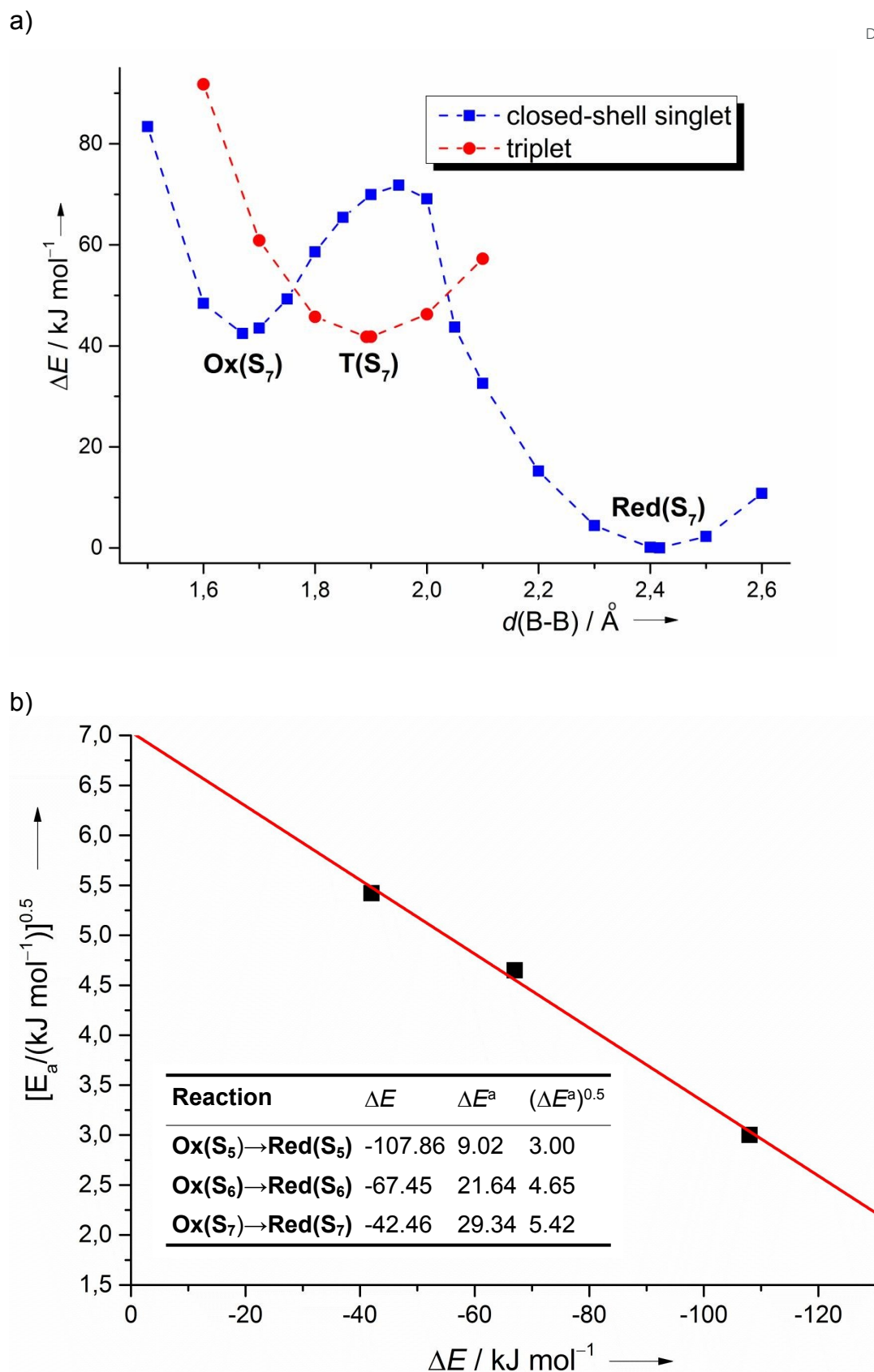


Figure 8. a) Calculated relative energy as a function of the B-B distance for the diborane complex with substrate **S₇**. b) Marcus-type plot of the square-root of the activation energy, $(\Delta E^a)^{0.5}$, as a function of the energy difference ΔE . The inserted table summarizes the estimated energy differences and activation energies (ΔE^a). All values are given in kJ mol^{-1} .

Experimental Details

All reactions were carried out under a dry Ar atmosphere by using standard Schlenk technique. The reagents 1,2-naphthalene-dione 9,10-phenanthrene-dione and 3,4,5,6-tetrachlorobenzoquinone were purchased from Sigma–Aldrich. The reagents benzil, 2,2'-dichlorobenzil and 1,2-acenaphthylene-dione were purchased from Fluka, Alfa Aesar and abcr. All reagents were used without further purification. The compound [(TfO)B(hpp)]₂ was synthesized according to the literature.^[22] All solvents were rigorously dried by the solvent purification system MB SPS-800 MBRAUN and stored over molecular sieves (4 Å) after being degassed by the freeze-pump-thaw method. Infrared spectra were recorded as KBr discs or as powder with a BIORAD Excalibur FTS 3000 and a Bruker Alpha Platinum-ATR. BRUKER Avance DPX 200, BRUKER Avance II 400 and BRUKER Avance III 600 devices were used for NMR spectroscopy. NMR spectra were recorded at 298 K and ¹¹B NMR chemical shifts are given in ppm relative to BF₃·Et₂O. Elemental analyses were performed at the Microanalytical Laboratory of the University of Heidelberg using the vario EL and vario MICRO cube devices from Elementar Analysensysteme GmbH. Mass spectra were obtained with JOEL JMS-700 magnetic sector and BRUKER ApexQe hybrid 9.4 T FT-ICR spectrometer at the MS laboratory of the University of Heidelberg. UV-Vis spectra were recorded at 298 K using a Varian Cary 5000 UV/Vis NIR spectrometer.

4(OTf)

In a dry argon-flushed Schlenk flask [(TfO)B(hpp)]₂ (**2**, 50 mg, 0.08 mmol) was dissolved in 1.0 mL of absolute dichloromethane. After cooling to –40 °C with a cooling bath a solution of 1,2-naphthalene-dione (**S**₃, 13 mg, 0.08 mmol) in 1.0 mL of absolute dichloromethane was added. The cooling bath was removed, and the reaction mixture stirred for 1 h at room temperature. The volume of the reaction mixture was reduced to an eighth of its original value and the solution stored at –20 °C. Colorless crystals precipitated after a few days. The mother liquor was removed with a syringe and the crystalline solid dried in vacuo to yield the product in a yield of 32 mg (0.04 mmol, 51%). C,H,N analysis (%) for C₂₆H₃₀B₂F₆N₆O₈S₂·CH₂Cl₂ (754.29 g mol⁻¹): calcd. C 38.64, H 3.84, N: 10.01; found C 38.05, H 3.93, N 10.06. ¹H NMR (400 MHz, CD₂Cl₂): δ = 8.07 (d, 1 H, ³J = 8 Hz, H_{arom}), 7.88 (d, 1 H, ³J = 8 Hz, H_{arom}),

7.58–7.49 (m, 3 H, H_{arom}), 7.40 (d, 1 H, ³J = 8 Hz, H_{arom}), 3.57–3.10 (m, 16 H, N-CH₂), 2.13–1.96 (m, 6 H, CH₂), 1.79–1.70 (m, 2 H, CH₂) ppm. ¹¹B NMR (128 MHz, CD₂Cl₂): δ = 6.52 (s, 1 B), 2.35 (s, 1 B, BOSO₂CF₃) ppm. ¹³C NMR (100 MHz, CD₂Cl₂): δ = 154.3 (C_q, hpp), 144.8 (C_{arom}-O), 137.9 (C_{arom}-O), 133.0 (C_{arom}), 128.7 (C_{arom}), 127.2 (C_{arom}), 127.0 (C_{arom}), 123.5 (C_{arom}), 121.4 (C_{arom}), 121.4 (SO₃CF₃), 117.4 (C_{arom}), 112.6 (C_{arom}), 48.4 (NCH₂), 48.2 (NCH₂), 40.5 (NCH₂), 40.0 (NCH₂), 21.5 (CH₂) ppm. ¹⁹F NMR (376 MHz, CD₂Cl₂): δ = -77.00 (s, BOSO₂CF₃), -78.94 (s, free SO₃CF₃⁻) ppm. MS (HR-ESI⁺): m/z (%) = 429.19 ([hppH]₂[SO₃CF₃]⁺, 100%). UV-Vis (CH₂Cl₂, c = 7.34 · 10⁻⁶ mol L⁻¹): λ (ε in L mol⁻¹ cm⁻¹) = 230 (8.45 · 10⁴), 285 (7.97 · 10³), 328 (4.73 · 10³) nm. IR (powder): $\tilde{\nu}$ = 2961(w), 2879(w), 1630(m), 1595(m), 1542(m), 1460(w), 1446(w), 1388(m), 1322(m), 1219(m), 1150(s), 1114(s), 1071(m), 1042(m), 1026(s), 1005(m), 953(s), 875(w), 799(m), 774(w), 760(w), 740(w), 698(w), 675(w), 635(s), 623(s), 601(m), 573(m), 514(m) cm⁻¹. Crystal data for **4**(OTf)·CH₂Cl₂, C₂₇H₃₂B₂Cl₂F₆N₆O₈S₂, M_r = 839.27, 0.541 x 0.466 x 0.336 mm, triclinic, space group P-1, a = 12.366(4), b = 13.352(5), c = 13.473(3) Å, α = 101.35°, β = 108.56°, γ = 117.56°, V = 1705.8(12) Å³, Z = 2, ρ_{calcd} = 1.634 Mg · m⁻³, Mo-K_α radiation (λ = 0.71073 Å), T = 120 K, θ_{range} = 2.410 - 29.990°. Reflections collected 9838, independent reflections 8515, R_{int} = 0.0408. Final R indices [I > 2σ(I)]: R = 0.0471, wR = 0.1180.

5(OTf)

In a dry argon-flushed Schlenk flask [(TfO)B(hpp)]₂ (**2**, 50 mg, 0.08 mmol) was dissolved in 1.0 mL of absolute dichloromethane. After cooling to -40 °C with a cooling bath a solution of 9,10-phenanthrene-dione (**S**₄, 17 mg, 0.08 mmol) in 1.0 mL of absolute dichloromethane was added. The cooling bath was removed, and the reaction mixture stirred for 1 h at room temperature. The volume of the reaction mixture was reduced to an eighth of its original value and the solution stored at -20 °C. Colorless crystals precipitated after a few days. The mother liquor was removed with a syringe and the crystalline solid dried in vacuo to yield the product in a yield of 35 mg (0.04 mmol, 52%). C,H,N analysis (%) for C₃₀H₃₂B₂F₆N₆O₈S₂ · 1.5 CH₂Cl₂ (804.35 g mol⁻¹): calcd. C 40.61, H 3.79, N: 9.02; found C 40.44, H 3.86, N 9.44. ¹H NMR (400 MHz, CD₂Cl₂): δ = 8.81–8.72 (m, 2 H, H_{arom}), 8.26–8.24 (m, 2 H, H_{arom}), 7.79–7.60 (m, 4 H, H_{arom}), 3.54–3.20 (m, 16 H, N-CH₂), 2.06–1.97 (m, 6 H, CH₂), 1.78–1.66 (m, 2 H, CH₂) ppm. ¹¹B NMR (128 MHz, CD₂Cl₂): δ = 6.58 (s, 1 B), 3.07 (s, 1 B, BOSO₂CF₃) ppm. ¹³C NMR (100 MHz,

CD₂Cl₂): δ = 151.5 (C_q, hpp), 139.7 (C_{arom}-O), 128.3 (C_{arom}-O), 128.0 (C_{arom}), 127.9 (C_{arom}), 127.8 (C_{arom}), 127.3 (C_{arom}), 127.6 (C_{arom}), 126.1 (C_{arom}), 125.2 (C_{arom}), 124.1 (C_{arom}), 123.9 (C_{arom}), 123.4 (C_{arom}), 122.9 (C_{arom}), 122.3 (C_{arom}), 120.6 (SO₃CF₃), 47.3 (NCH₂), 38.5 (NCH₂), 21.0 (CH₂) ppm. ¹⁹F NMR (376 MHz, CD₂Cl₂): δ = -77.03 (s, BOSO₂CF₃), -79.00 (s, free SO₃CF₃⁻) ppm. MS (HR-ESI⁺): m/z (%) = 429.19 ([hppH]₂[SO₃CF₃]⁺, 2%). UV-Vis (CH₂Cl₂, c = 2.09·10⁻⁵ mol L⁻¹): λ (ϵ in L mol⁻¹ cm⁻¹) = 257 (3.53·10⁴), 307 (7.36·10³), 345 (9.91·10²), 361 (1.01·10³) nm. IR (KBr disk): $\tilde{\nu}$ = 2957(w), 2882(w), 1633(m), 1601(m), 1552(m), 1449(m), 1393(m), 1357(m), 1325(s), 1271(s), 1224(s), 1152(s), 1118(m), 1078(m), 1062(m), 1030(s), 977(m), 947(m), 803(w), 757(m), 724(m), 669(w), 638(s), 600(w), 573(w), 517(m) cm⁻¹. Crystal data for 5(OTf)·CH₂Cl₂, C₃₁H₃₄B₂Cl₂F₆N₆O₈S₂, M_r = 889.28, 0.40 x 0.40 x 0.40 mm, triclinic, space group P $\bar{1}$, a = 11.882(2), b = 12.192(2), c = 14.297(3) Å, α = 83.12°, β = 77.39°, γ = 75.38°, V = 1951.2(8) Å³, Z = 2, ρ_{calcd} = 1.514 Mg·m⁻³, Mo-K α radiation (λ = 0.71073 Å), T = 120 K, θ_{range} = 1.730 - 28.000°. Reflections collected 9387, independent reflections 6947, R_{int} = 0.0420. Final R indices [I > 2 σ (I)]: R = 0.0807, wR = 0.1906.

6(OTf)

In a dry argon-flushed Schlenk flask [(TfO)B(hpp)]₂ (**2**, 50 mg, 0.08 mmol) was dissolved in 1.0 mL of absolute dichloromethane. After cooling to -40 °C with a cooling bath a solution of 3,4,5,6-tetrachloro-*o*-benzoquinone (**S**₂, 19 mg, 0.08 mmol) in 0.5 mL of absolute dichloromethane was added. The cooling bath was removed, and the reaction mixture stirred for 1 h at room temperature. The solvent was removed and the solid was dried in vacuo to yield 36 mg of the product (0.04 mmol, 48%). C,H,N analysis (%) for C₂₂H₂₄B₂Cl₄F₆N₆O₈S₂ (842.00 g mol⁻¹): calcd. C 31.38, H 2.87, N: 9.98; found C 30.53, H 3.62, N 9.83. ¹H NMR (400 MHz, CD₂Cl₂): δ = 3.44–3.28 (m, 16 H, N-CH₂), 2.09–1.88 (m, 8 H, CH₂) ppm. ¹¹B NMR (128 MHz, CD₂Cl₂): δ = 7.22 (s, 1 B), 2.86 (s, 1 B, BOSO₂CF₃) ppm. ¹³C NMR (100 MHz, CD₂Cl₂): δ = 154.0 (C_q, hpp), 141.4 (C_{arom}-O), 139.4 (C_{arom}-O), 137.1 (C_{arom}), 129.1 (C_{arom}), 125.7 (C_{arom}), 122.0 (SO₃CF₃), 118.5 (C_{arom}), 48.2 (NCH₂), 48.0 (NCH₂), 40.6 (NCH₂), 39.9 (NCH₂), 21.4 (CH₂), 20.9 (CH₂) ppm. ¹⁹F NMR (376 MHz, CD₂Cl₂): δ = -77.10 (s, BOSO₂CF₃), -78.97 (s, free SO₃CF₃⁻) ppm. MS (HR-ESI⁺): m/z (%) = 429.19 ([hppH]₂[OTf]⁺, 100%). UV-Vis (CH₂Cl₂, c = 7.36·10⁻⁵ mol L⁻¹): λ (ϵ in L mol⁻¹ cm⁻¹) = 228 (7.85·10³), 298 (1.37·10³) nm. IR (KBr disk): $\tilde{\nu}$ = 2954(w), 2885(w),

1629(s), 1604(m), 1548(m), 1457(m), 1408(m), 1388(m), 1325(s), 1265(s), 1224(s), 1153(m), 1114(m), 1070(m), 1031(s), 1005(m), 952(m), 810(w), 797(w), 678(w), 638(s), 605(w), 574(w), 517(m) cm^{-1} .

Details of the XRD studies. Suitable crystals for single-crystal structure determination were taken directly from the mother liquor, taken up in perfluorinated polyether oil and fixed on a cryo loop. Full shells of intensity data were collected at low temperature with a Nonius Kappa CCD diffractometer (MoK α radiation, sealed X-ray tube, graphite monochromator) and a Bruker D8 Venture, dual source (Mo- or Cu-K α radiation, microfocus X-ray tube, Photon III Detector). Data were processed with the standard Nonius [28] and APEX3 [29] software. Multiscan absorption correction was applied using the SADABS program.[30] The structures were solved by intrinsic phasing and refined using the SHELXTL software package (Version 2014/6 and 2018/3).[31] Graphical handling of the structural data during solution and refinement was performed with XPMA and OLEX2.[32] All nonhydrogen atoms were given anisotropic displacement parameters. Hydrogen atoms were generally set at calculated positions and refined with a riding model. CCDC 1944030 (**4**(OTf)), 1944027 (**5**(OTf)), 1944028 (C₂₀H₁₆BCl₁₀N₃O₄), and 1944029 (C₂₂H₂₄F₃N₃O₄S) contain the supplementary crystallographic data for this paper.

Details of the quantum-chemical calculations. DFT calculations were performed with the TURBOMOLE [33,34,35] or ORCA 4.4.1 [36] program packages. The B3LYP functional [37,38] was used in combination with the def2-TZVP basis set.[39] For the calculation of the ¹¹B NMR shifts the BP86 functional [40] was used in combination with the def2-SV(P) basis set.[41] The structures were visualized with the Diamond 3.0 software.[42]

Conflicts of interest

There are no conflicts of interest to declare.

Acknowledgements

View Article Online
DOI: 10.1039/C9DT03151K

The authors gratefully acknowledge financial support by the *Deutsche Forschungsgemeinschaft* (DFG).

-
- [1] E. C. Neeve, S. J. Geier, I. A. I. Mkhaliid, S. A. Westcott, T. B. Marder, *Chem. Rev.*, 2016, **116**, 9091–9161.
- [2] H.-J. Himmel, *Eur. J. Inorg. Chem.*, 2018, 2139–2154.
- [3] a) N. Tsukahara, H. Asakawa, K.-H. Lee, Z. Lin, M. Yamashita, *J. Am. Chem. Soc.*, 2017, **139**, 2593–2596; b) Y. Katsuma, N. Tsukahara, L. Wu, Z. Lin, M. Yamashita, *Angew. Chem.*, 2018, **130**, 6217–6222; *Angew. Chem. Int. Ed.*, 2018, **57**, 6109–6114; c) Y. Katsuma, L. Wu, Z. Lin, S. Akiyama, M. Yamashita, *Angew. Chem.*, 2019, **131**, 323–327; *Angew. Chem. Int. Ed.*, 2019, **58**, 317–321.
- [4] a) H. Asakawa, K.-H. Lee, Z. Lin, M. Yamashita, *Nat. Commun.*, 2014, **5**, 4245–4253; b) H. Asakawa, K.-H. Lee, K. Furukawa, Z. Lin, M. Yamashita, *Chem. Eur. J.*, 2015, **21**, 4267–4271; c) Y. Katsuma, H. Asakawa, K.-H. Lee, Z. Lin, M. Yamashita, *Organometallics*, 2016, **35**, 2563–2566; d) Y. Katsuma, H. Asakawa, M. Yamashita, *Chem. Sci.*, 2018, **9**, 1301–1310.
- [5] S. Akiyama, K. Yamada, M. Yamashita, *Angew. Chem. Int. Ed.*, 2019, **58**, in press (DOI: 10.1002/anie.201907400).
- [6] J. Landmann, J. A. P. Sprenger, M. Hailmann, V. Bernhardt-Pitchougina, H. Willner, N. Ignat'ev, E. Bernhardt, M. Finze, *Angew. Chem.*, 2015, **127**, 11411–11416; *Angew. Chem. Int. Ed.*, 2015, **54**, 11259–11264.
- [7] A. Hübner, T. Kaese, M. Diefenbach, B. Endeward, M. Bolte, H.-W. Lerner, M. C. Holthausen, M. Wagner, *J. Am. Chem. Soc.*, 2015, **137**, 3705–3714.
- [8] W. J. Grigsby, P. P. Power, *J. Am. Chem. Soc.*, 1996, **118**, 7981–7988.
- [9] Y. Shoji, T. Matsuo, D. Hashizume, M. J. Gutmann, H. Fueno, K. Tanaka, K. Tamao, *J. Am. Chem. Soc.*, 2011, **133**, 11058–11061.
- [10] W. Preetz, B. Steuer, *Z. Naturforsch. B: J. Chem. Sci.*, 1996, **51**, 551–556.
- [11] G. Bélanger-Chabot, H. Braunschweig, *Angew. Chem. Int. Ed.* 2019, in press (DOI: 10.1002/anie.201906666).
- [12] M. Arrowsmith, J. Böhnke, H. Braunschweig, A. Deißenberg, R. D. Dewhurst, W. C. Ewing, C. Hörl, J. Mies, J. H. Muessig, *Chem. Commun.*, 2017, **53**, 8265–8267.

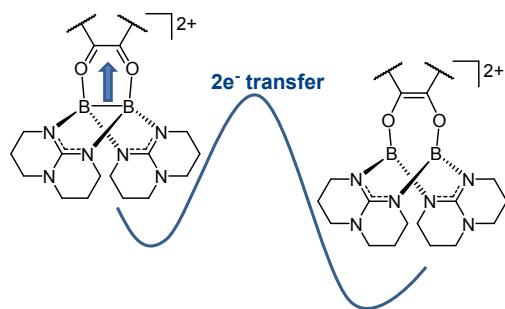
- [13] R. D. Dewhurst, E. C. Neeve, H. Braunschweig, T. B. Marder, *Chem. Commun.*, 2015, **51**, 9594–9607.
- [14] a) W. Clegg, C. Dai, F. J. Lawlor, T. B. Marder, P. Nguyen, N. C. Norman, N. L. Pickett, W. P. Power, A. J. Scott, *J. Chem. Soc., Dalton Trans.*, 1997, 839–846; b) S. Pietsch, U. Paul, I. A Cade, M. J. Ingleson, U. Radius, T. B. Marder, *Chem. Eur. J.*, 2015, **21**, 9018–9021; c) M. Eck, S. Wuertemberger-Pietsch, A. Eichhorn, J. H. J. Berthel, R. Bertermann, U. S. D. Paul, H. Schneider, A. Friedrich, C. Kleeberg, U. Radius, T. B. Marder, *Dalton Trans.*, 2017, **46**, 3661–3680.
- [15] S. Pietsch, E. C. Neeve, D. C. Apperley, R. Bertermann, F. Mo, D. Qiu, M. S. Cheung, L. Dang, J. Wang, U. Radius, Z. Lin, C. Kleeberg, T. B. Marder, *Chem. Eur. J.*, 2015, **21**, 7082–7099.
- [16] a) A.-F. Pécharman, A. L. Colebatch, M. S. Hill, C. L. McMullin, M. F. Mahon, C. Weetman, *Nat. Commun.*, 2017, **8**, 15022–15028; b) A.-F. Pécharman, M. S. Hill, M. F. Mahon, *Dalton Trans.*, 2018, **47**, 7300–7305; c) A.-F. Pécharman, M. S. Hill, C. L. McMullin, M. F. Mahon, *Organometallics*, 2018, **37**, 4457–4464; d) A.-F. Pécharman, M. S. Hill, G. McMullon, C. L. McMullin, M. F. Mahon, *Chem. Sci.*, 2019, **10**, 6672–6682.
- [17] A.-F. Pécharman, M. S. Hill, M. F. Mahon, *Angew. Chem.*, 2018, **130**, 10848–10851; *Angew. Chem. Int. Ed.*, 2018, **57**, 10688–10691.
- [18] a) O. Ciobanu, E. Kaifer, M. Enders, H.-J. Himmel, *Angew. Chem.*, 2009, **121**, 5646–5649; *Angew. Chem. Int. Ed.*, 2009, **48**, 5538–5541; b) N. Schulenberg, O. Ciobanu, E. Kaifer, H. Wadepohl, H.-J. Himmel, *Eur. J. Inorg. Chem.*, 2010, 5201–5210; c) A. Wagner, S. Litters, J. Elias, E. Kaifer, H.-J. Himmel, *Chem. Eur. J.*, 2014, **20**, 12514–12527.
- [19] a) M. Frick, E. Kaifer, H.-J. Himmel, *Angew. Chem.*, 2017, **129**, 11804–11807; *Angew. Chem. Int. Ed.*, 2017, **56**, 11645–11648; b) M. Frick, J. Horn, H. Wadepohl, E. Kaifer, H.-J. Himmel, *Chem. Eur. J.*, 2018, **24**, 16983–16986.
- [20] a) S. Litters, M. Enders, E. Kaifer, H.-J. Himmel, *Nat. Chem.*, 2013, **5**, 1029–1034; b) S. Litters, E. Kaifer, H.-J. Himmel, *Angew. Chem.*, 2016, **128**, 4417–4420; *Angew. Chem. Int. Ed.*, 2016, **55**, 4345–4347; c) S. Litters, E. Kaifer, H.-J. Himmel, *Eur. J. Inorg. Chem.*, 2016, 4090–4098.
- [21] H.-J. Himmel, *Angew. Chem.*, 2019, **131**, 11724–11742; *Angew. Chem. Int. Ed.*, 2019, **58**, 11600–11617.

- [22] J. Horn, A. Widera, S. Litters, E. Kaifer, H.-J. Himmel, *Dalton Trans.*, 2018, **47**, 2009–2017.
- [23] A. Widera, H. Wadepohl, H.-J. Himmel, *Angew. Chem.*, 2019, **131**, 5957–5961; *Angew. Chem. Int. Ed.*, 2019, **58**, 5897–5901.
- [24] A. Widera, D. Vogler, H. Wadepohl, E. Kaifer, H.-J. Himmel, *Angew. Chem.*, 2018, **130**, 11627–11630; *Angew. Chem. Int. Ed.*, 2018, **57**, 11456–11459.
- [25] a) M. T. Huynh, C. W. Anson, A. C. Cavell, S. S. Stahl, S. Hammes-Schiffer, *J. Am. Chem. Soc.*, 2016, **138**, 15903–15910; b) M. Hanif, L. Ping, G. Cheng, W. Zhi-ming, Y. Shi-min, Y. Bing, W. Chun-Lei, M. Yu-guang, *Chem. Res. Chinese Univ.*, 2009, **25**, 950–956; c) I. P. Romanova, A. V. Bogdanov, V. F. Mironov, O. A. Larionova, S. K. Latypov, A. A. Balandina, D. G. Yakhvarov, O. G. Sinyashin, *Mendeleev Commun.*, 2009, **19**, 306–308.
- [26] O. Ciobanu, P. Roquette, S. Leingang, H. Wadepohl, J. Mautz, H.-J. Himmel, *Eur. J. Inorg. Chem.*, 2007, 4530–4534.
- [27] C. Feuvrie, I. Ledoux, J. Zyss, H. Le Bozec, O. Maury, *C. R. Chimie*, 2005, **8**, 1243–1248.
- [28] DENZO-SMN: Z. Otwinowski & W. Minor, Processing of X-ray Diffraction Data Collected in Oscillation Mode, *Methods Enzymol.*, 1997, **276**, Eds C. W. Carter R. M. Sweet, Academic Press.
- [29] APEX3 software package, Bruker AXS, 2016.
- [30] a) G. M. Sheldrick, SADABS, Program for Empirical Absorption Correction, University of Göttingen, Germany; b) G. M. Sheldrick, SADABS, Bruker AXS GmbH, Karlsruhe, Germany, 2004–2014; c) L. Krause, R. Herbst-Irmer, G. M. Sheldrick, D. Stalke, *J. Appl. Cryst.*, 2015, **48**, 3.
- [31] a) G. M. Sheldrick, SHELXT, Program for Crystal Structure Solution, University of Göttingen, Germany, 2014–2018; b) G. M. Sheldrick, *Acta Crystallogr. Sect. A*, 2015, **71**, 3–8.
- [32] a) O. V. Dolomanov, L. J. Bourhis, R. J. Gildea, J. A. K. Howard, H. Puschmann, OLEX2: A complete structure solution, refinement and analysis program, *J. Appl. Cryst.* 2009, **42**, 339–341; b) P. v. d. Sluis, A. L. Spek, *Acta Cryst. A*, 1990, **46**, 194; c) A. L. Spek, *Acta Cryst. C*, 2015, **71**, 9.
- [33] TURBOMOLE V7.2 2017, a development of University of Karlsruhe and Forschungszentrum Karlsruhe GmbH, 1989–2007, TURBOMOLE GmbH, since 2007; available from <http://www.turbomole.com>.

- [34] R. Ahlrichs, M. Bär, M. Häser, H. Horn, C. Kölmel, *Chem. Phys. Lett.*, 1989, **162**, 165–169.
- [35] O. Treutler, R. Ahlrichs, *J. Chem. Phys.*, 1995, **102**, 346–354.
- [36] ORCA V4.4.1, Mühlheim a. d. Ruhr, Germany, 2017.
- [37] A. D. Becke, *J. Chem. Phys.*, 1993, **98**, 5648–5652.
- [38] P. J. Stephens, F. J. Devlin, C. F. Chabalowski, M. J. Frisch, *J. Phys. Chem.*, 1994, **98**, 11623–11627.
- [39] F. Weigend, R. Ahlrichs, *Phys. Chem. Chem. Phys.*, 2005, **7**, 3297–3305.
- [40] a) A. D. Becke, *Phys. Rev. A*, 1988, **38**, 3098–3100; b) J. P. Perdew, *Phys. Rev. B*, 1986, **33**, 8822–8824.
- [41] D. Andrae, U. Haeussermann, M. Dolg, H. Stoll, H. Preuss, *Theor. Chim. Acta*, 1990, **77**, 123–141.
- [42] Diamond V3.0, Bonn, Germany, 1997–2004.

TOC entry

The complexation and reduction of a series of diones with different redox-potentials at a dicationic diborane are analysed.



Electron transfer in complexes of B^{II} cations with organic π -acceptors: A combined experimental and quantum-chemical study

D. Vogler, N. Wolf, E. Kaifer, H.-J. Himmel*

Keywords: boron, diborane, reduction, electron-transfer, boron-boron bond